Methods

We sample electron emission from atoms using the experimental set-up that was described in detail[1] and employed recently for probing Auger electrons on a few-fs timescale[22]. The essential innovation here is that waveform-controlled few-cycle light now provides a reproducible excitation burst for accurate triggering and a reproducible streaking field for capturing sub-fs electron emission from atoms. For excitation, XUV bursts are produced from Ne atoms ionized by intense, few-cycle waveform-controlled light pulses[5] in a process giving rise to high-order harmonics of the incident light for periodic (multi-cycle) pumping[10,11]. The collinear XUV and laser beams are focused into a neon gas jet and delayed with respect to each other for the ATR measurements with a two-component Mo/Si broadband multilayer mirror[1] (radius of curvature = −70 mm) placed 2.5 m downstream from the source. The internal part of the laser beam (~3 mm in diameter) was blocked with a zirconium filter (transmitting the XUV pulse) in front of the Mo/Si mirror. The resultant annular laser beam (with a dark spot 3 mm in diameter in its centre) and the XUV beam (~3 mm in diameter) confined by the annular laser beam were focused by the external and internal sections of the two-component Mo/Si mirror[1], respectively. The two components can be aligned separately and translated with respect to each other along the optical axis of the mirror.

The reflectivity band of the multilayer extends from 85 V to 100 V with a peak reflectance of ~30% and a FWHM of ~9 V. Electrons ejected following the XUV excitation are collected within a narrow cone (<4°) aligned parallel to the laser and XUV polarization and analysed with a time-of-flight spectrometer. Two types of experiments have been implemented. First, by removing the zirconium filter we used the internal part of the Mo/Si mirror to focus both the XUV and the laser beam to eliminate any external source of fluctuations in the timing between the excitation and probing pulses (results summarized in Fig. 3). In the second type of studies, the XUV and the laser beam were reflected by different sections of the focusing mirror as described above. In these investigations the probing laser field could be delayed with respect to the XUV excitation pulse by the translation of the internal part of the mirror on a nanometre scale, yielding the data shown in Figs 4 and 5.

Received 24 October; accepted 5 December 2003; doi:10.1038/nature02277.

1. Hentschel, M. *et al.* Attosecond metrology. *Nature* **414,** 509–513 (2001).
2. Zewail, A. Femtochemistry: atomic-scale dynamics of the chemical bond (adapted from the Nobel Lecture). *J. Phys. Chem. A* **104,** 5660–5694 (2000).
3. Itatani, J. *et al.* Attosecond streak camera. *Phys. Rev. Lett.* **88,** 173903 (2002).
4. Kitzler, M., Milosevic, N., Scrinzi, A., Krausz, F. & Brabec, T. Quantum theory of attosecond XUV pulse measurement by laser-dressed photoionization. *Phys. Rev. Lett.* **88,** 173904 (2002).
5. Baltuska, A. *et al.* Attosecond control of electronic processes by intense light fields. *Nature* **421,** 611–615 (2003).
6. Bradley, D. J., Liddy, B. & Sleat, W. E. Direct linear measurement of ultrashort light pulses with a picosecond streak camera. *Opt. Commun.* **2,** 391 (1971).
7. Schelev, M. Ya., Richardson, M. C. & Alcock, A. J. Image-converter streak camera with picosecond resolution. *Appl. Phys. Lett.* **18,** 354 (1971).
8. Kane, D. J. & Trebino, R. Characterization of arbitrary femtosecond pulses using frequency-resolved optical gating. *IEEE J. Quantum Electron.* **29,** 571–579 (1993).
9. Sekikawa, T., Katsura, T., Miura, S. & Watanabe, S. Measurement of the intensity-dependent atomic dipole phase of a high harmonic by frequency-resolved optical gating. *Phys. Rev. Lett.* **88,** 193902 (2002).
10. L'Huillier, A. & Balcou, Ph. High-order harmonic generation in rare gases with a 1-ps 1053-nm laser. *Phys. Rev. Lett.* **70,** 774–777 (1993).
11. Macklin, J. J., Kmetec, J. D. & Gordon, C. L. III High-order harmonic generation using intense femtosecond pulses. *Phys. Rev. Lett.* **70,** 766–769 (1993).
12. Schafer, K. J., Yang, B., DiMauro, L. F. & Kulander, K. C. Above threshold ionization beyond the high harmonic cutoff. *Phys. Rev. Lett.* **70,** 1599–1602 (1993).
13. Corkum, P. B. Plasma perspective on strong-field multiphoton ionization. *Phys. Rev. Lett.* **71,** 1994–1997 (1993).
14. Lewenstein, M., Balcou, Ph., Ivanov, M. Yu., L'Huillier, A. & Corkum, P. B. Theory of high-harmonic generation by low-frequency laser fields. *Phys. Rev. A* **49,** 2117–2132 (1994).
15. Christov, I. P., Murnane, M. M. & Kapteyn, H. C. High-harmonic generation of attosecond pulses in the "single-cycle" regime. *Phys. Rev. Lett.* **78,** 1251–1254 (1997).
16. Kan, C., Burnett, N. H., Capjack, C. E. & Rankin, R. Coherent XUV generation from gases ionized by several cycle optical pulses. *Phys. Rev. Lett.* **79,** 2971–2974 (1997).
17. de Bohan, A., Antoine, P., Milosevic, D. B. & Piraux, B. Phase-dependent harmonic emission with ultrashort laser pulses. *Phys. Rev. Lett.* **81,** 1837–1840 (1998).
18. Tempea, G., Geissler, M. & Brabec, T. Phase sensitivity of high-order harmonic generation with few-cycle laser pulses. *J. Opt. Soc. Am. B* **16,** 669–674 (1999).
19. Paul, P. M. *et al.* Observation of a train of attosecond pulses from high harmonic generation. *Science* **292,** 1689–1692 (2001).
20. Mairesse, Y. *et al.* Attosecond synchronisation of high-harmonic soft X-rays. *Science* **302,** 1540–1543 (2003).
21. Tzallas, P., Charalambidis, D., Papadogiannis, N. A., Witte, K. & Tsakiris, G. D. Direct observation of attosecond light bunching. *Nature* **426,** 267–271 (2003).
22. Drescher, M. *et al.* Time-resolved atomic inner-shell spectroscopy. *Nature* **419,** 803–807 (2002).

Acknowledgements This work was sponsored by the Fonds zur Förderung der wissenschaftlichen Forschung (Austria), the Deutsche Forschungsgemeinschaft and the Volkswagenstiftung (Germany) and by the European Union's Human Potential Programme.

Competing interests statement The authors declare that they have no competing financial interests.

Correspondence and requests for materials should be addressed to F.K. (ferenc.krausz@tuwien.ac.at).

Giant magnetoresistance in organic spin-valves

Z. H. Xiong, Di Wu, Z. Valy Vardeny & Jing Shi

Department of Physics, University of Utah, Salt Lake City, Utah 84112, USA

A spin valve is a layered structure of magnetic and non-magnetic (spacer) materials whose electrical resistance depends on the spin state of electrons passing through the device and so can be controlled by an external magnetic field. The discoveries of giant magnetoresistance[1] and tunnelling magnetoresistance[2] in metallic spin valves have revolutionized applications such as magnetic recording and memory, and launched the new field of spin electronics[3]—'spintronics'. Intense research efforts are now devoted to extending these spin-dependent effects to semiconductor materials. But while there have been noteworthy advances in spin injection and detection using inorganic semiconductors[4–6], spin-valve devices with semiconducting spacers have not yet been demonstrated. π-conjugated organic semiconductors may offer a promising alternative approach to semiconductor spintronics, by virtue of their relatively strong electron–phonon coupling[7] and large spin coherence[8]. Here we report the injection, transport and detection of spin-polarized carriers using an organic semiconductor as the spacer layer in a spin-valve structure, yielding low-temperature giant magnetoresistance effects as large as 40 per cent.

π-conjugated organic semiconductors (OSEs) are a relatively new class of electronic materials that are revolutionizing important technological applications including information display[9] (ref. 10 and references therein) and large-area electronics (ref. 11 and references therein), owing to their ability to be economically processed in large areas, their compatibility with low-temperature processing, the tunability of their electronic properties, and the simplicity of thin-film device fabrication. The virtually limitless flexibility of synthetic organic chemistry allows the fabrication of π-conjugated OSE structures with a degree of control unattainable with the conventional inorganic semiconductors. In addition, the OSEs have extremely weak spin-orbit interaction and weak hyperfine interaction, so that electron spin diffusion length is especially long[8]. These properties make them ideal for spin-polarized electron injection and transport applications.

Here we have chosen the small π-conjugated molecule 8-hydroxy-quinoline aluminium (Alq_3), most commonly used in organic light-emitting diodes (OLEDs)[10], to serve as an OSE spacer in organic spin-valves, because it can easily be deposited as thin films and integrated with a variety of metallic electrodes. As shown in Fig. 1a, the vertical organic spin-valves that we fabricated consist of three layers: two ferromagnetic electrode films (FM_1 and FM_2, respectively) and the OSE spacer. By engineering the two FM electrodes to have different coercive fields (H_{c1} and H_{c2}, respectively), their magnetization directions can have either a parallel or anti-parallel alignment configuration when sweeping the external magnetic field, H; this is essential for proving the spin-valve effect.

Intrigued by the possibility of spin-injection involving a π-conjugated OSE oligomer (sexi-thiophene, T_6)[12], where both the opposite FM electrodes were $La_{0.67}Sr_{0.33}MnO_3$ (LSMO), we have chosen LSMO for the bottom electrode (FM_1) and cobalt as the top electrode (FM_2) in our devices (Fig. 1a, b). LSMO is believed to be a half-metallic ferromagnet that possesses near-100% spin-polarization[13]. We note that unlike metallic FM films such as cobalt, nickel, iron or their alloys, the LSMO films are already stable against oxidation. In fact, our LSMO films have been cleaned and re-used

many times without any apparent degradation. After neat cleaning using acetone, the LSMO was introduced into the evaporation chamber with a base pressure of 5×10^{-7} torr, where the OSE film (Alq_3) was thermally evaporated. Without breaking the vacuum, we then deposited a thin (3–6 nm) cobalt (Co) film followed by an aluminium (Al) contact, using a shadow mask. The obtained active device area was about $2 \times 3\ mm^2$. We have fabricated several spin-valve devices with various OSE thicknesses d, between 130 to 250 nm. The OSE thickness was measured by an *in situ* thickness monitor and independently confirmed outside the chamber by scanning electron microscopy and thickness profilometry, respectively.

A schematic band diagram of a typical LSMO/Alq_3/Co device is shown in Fig. 1c. In the rigid band approximation—that is, without taking into account the relaxation and polarization energy associated with charge injection—the highest occupied molecular orbital (HOMO) of Alq_3 lies about 0.9 eV below the Fermi levels, E_F, of the FM electrodes, whereas the lowest unoccupied molecular orbital (LUMO) lies about 2.00 eV above E_F (refs 14, 15). At low applied bias voltages V, holes are injected from the anode into the HOMO level of the OSE mainly by tunnelling through the bottom potential barrier. In addition, the similar work function value ϕ of the two electrodes (Fig. 1c) leads to a symmetric current–voltage I–V response (Fig. 1d). For fabricated devices with $d > 100$ nm we found that the I–V characteristic was nonlinear with a weak temperature dependence (Fig. 1d), indicative of carrier injection by tunnelling. Control devices with similar OSE thickness, in which ITO replaced the LSMO bottom electrode, showed electroluminescence and also a conductivity detected magnetic resonance at $g \approx 2$ (see Supplementary Information), indicating carrier injection into the OSE. In addition, at low V we measured a typical resistance of 10^4–$10^5\ \Omega$ that depends on the deposition rate and thickness of the Co electrode; such resistance is also consistent with a dominant pinhole-free organic spacer. Devices with $d < 100$ nm, however, showed a linear I–V response and lack of both conductivity detected magnetic resonance and electroluminescence, leading us to believe that these devices have an 'ill-defined' layer of up to 100 nm that may contain pinholes and Co inclusions. These findings suggest that the OSE spacers in the spin-valve devices fabricated with $d > 100$ nm may be composed of two sublayers: one sublayer with a thickness d_0 of the order of 100 nm immediately below the Co electrode that contains Co inclusions owing to the interdiffusion; and a second sublayer of neatly deposited Alq_3 between this defected sublayer and the LSMO film, having a thickness $d - d_0$, in which carrier transport is dominated by carrier drift.

The magnetoresistance of the fabricated devices was measured in a closed-cycle refrigerator from 11 to 300 K by sending a current through the two interfaces, while varying an external in-plane magnetic field, H (Fig. 1a). The hysteresis loops of the magnetization versus H for the FM electrodes were measured by

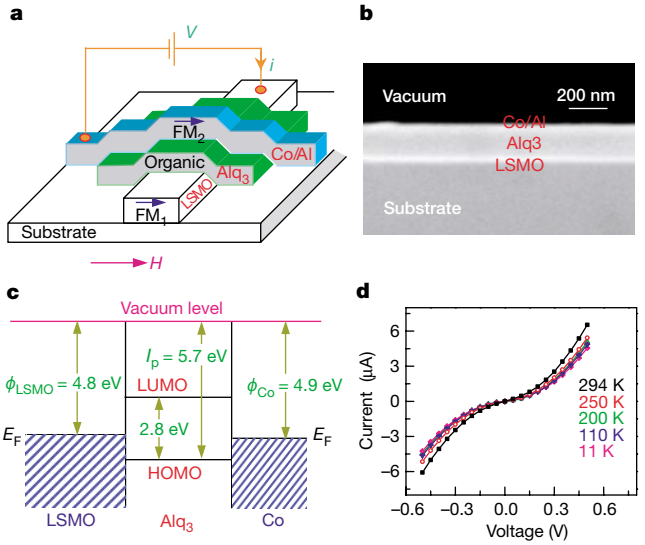

Figure 1 The structure and transport properties of the fabricated organic spin-valve devices. **a**, Schematic representation of a typical device that consists of two FM electrodes (FM_1 and FM_2) and an OSE spacer. Spin-polarized electrical current I flows from FM_1 (LSMO), through the OSE spacer (Alq_3), to FM_2 (Co) when a positive bias V is applied. An in-plane magnetic field, H, is swept to switch the magnetization directions of the two FM electrodes separately. **b**, Scanning electron micrograph of a functional organic spin-valve consisting of a 60-monolayer-thick LSMO film, a 160-nm-thick Alq_3 spacer, a 3.5-nm-thick Co electrode and a 35-nm-thick Al electrode. **c**, Schematic band diagram of the OSE device in the rigid band approximation showing the Fermi levels and the work functions of the two FM electrodes, LSMO and Co, respectively, and the HOMO–LUMO levels of Alq_3. **d**, I–V response of the organic spin-valve device with $d = 200$ nm at several temperatures.

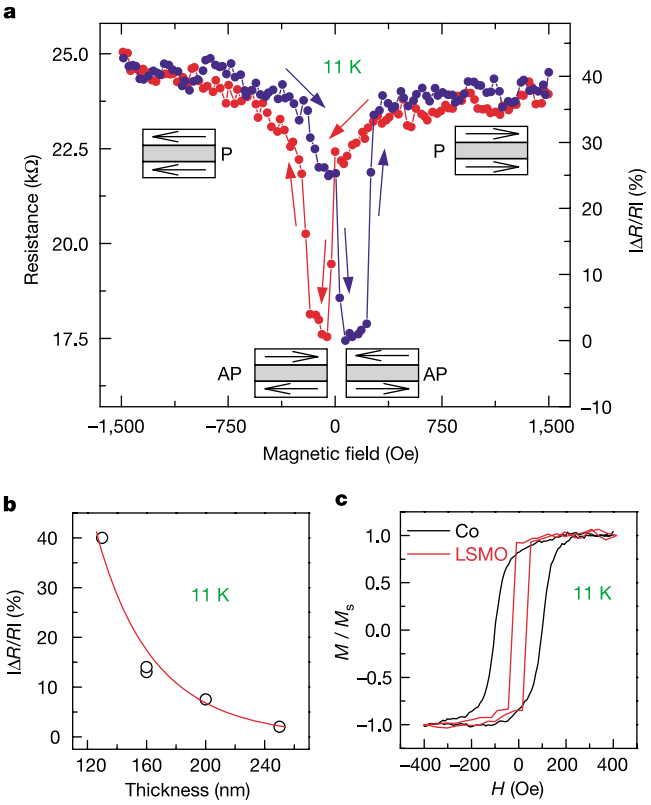

Figure 2 The magneto-transport response of the OSE spin-valve devices. **a**, GMR loop of a LSMO (100 nm)/Alq_3 (130 nm)/Co (3.5 nm) spin-valve device measured at 11 K. The blue (red) curve denotes GMR measurements made while increasing (decreasing) H. The anti-parallel (AP) and parallel (P) configurations of the FM magnetization orientations are shown in the insets at low and high H, respectively. The electrical resistance of the device is higher when the magnetization directions in FM_1 and FM_2 films are parallel to each other. **b**, The GMR value of a series of LSMO/Alq_3/Co devices with different d. The line fit through the data points was obtained using the spin diffusion model, equation (1), with three adjustable parameters, as explained in the text. All devices were fabricated on the same LSMO film. **c**, Magnetic hysteresis loops measured using MOKE for the LSMO electrode ($H_{c1} \approx 30$ Oe), and Co film deposited on Alq_3 under the same conditions as that for the Co electrode in the actual spin-valve devices ($H_{c2} \approx 150$ Oe). These coercive fields are seen in **a** when the resistance switches from parallel to the anti-parallel configuration, and vice versa.

the magneto-optic Kerr effect (MOKE) over the same temperature range. For comparison, we also measured separately the magnetoresistance (ΔR) of each FM electrode, as well as the OSE spacer on a variety of fabricated control devices: in all cases we found ΔR to be extremely small (less than 0.1% of the ΔR in the spin-valve devices) and devoid of any hysteresis with H (see Supplementary Information).

Figure 2a shows a typical magnetoresistance loop obtained in an LSMO/Alq_3/Co spin-valve device with $d = 130$ nm; the magnetoresistance curves of three other devices having larger d are shown in the Supplementary Information and their $\Delta R/R$ is summarized in Fig. 2b. A sizeable $\Delta R/R$ of 40%, which is a giant magnetoresistance (GMR) response comparable to that obtained in metallic GMR spin-valves[1,16], is observed at 11 K. The GMR of the devices with larger d is progressively smaller, but still measurable up to $d = 250$ nm (Fig. 2b). MOKE measurements performed on the LSMO bottom electrode of the device in Fig. 1a indicate that the coercive field of the LSMO film is $H_{c1} \approx 30$ Oe at 11 K (Fig. 2c). Although the top Co electrode of this device is not accessible to MOKE owing to the Al top contact, the coercive field of a Co film of the same thickness deposited on Alq_3 under similar conditions was nevertheless measured to be $H_{c2} \approx 150$ Oe at 11 K, much greater than that of the LSMO. Clearly then, the magnetization orientations in the two FM electrodes are anti-parallel to each other when the external field H is between H_{c1} and H_{c2}; in contrast, the magnetization orientations are parallel to each other when the field strength $H > H_{c2}$ (Fig. 2a insets). Therefore, the observed GMR hysteresis is undoubtedly due to the spin-valve effect. We note that the resistance in the anti-parallel alignment is lower than that in the parallel alignment, which is opposite to the spin-valve effect usually obtained using two identical FM electrodes, or two different 'd-band' metallic FM electrodes in some devices[16]. This 'inverse magnetoresistance' was also previously seen in LSMO/$SrTiO_3$/Co (ref. 17) and LSMO/$Ce_{0.69}La_{0.31}O_{1.845}$/Co (ref. 18) magnetic tunnel junction devices having extremely thin insulating spacers (~2 nm). The inverse magnetoresistance is believed to originate from the negative spin polarization of the Co d-band, in which the density-of-states of the majority-spin sub-band at the Fermi level is smaller than that of the minority-spin sub-band.

We may analyse the obtained GMR effect and its dependence on d using a simple injection and diffusion model. In conventional magnetic tunnel junction devices with a very thin insulating tunnel barrier, the Jullière model[19] has often been used to analyse the tunnelling magnetoresistance. In the present organic spin-valves, the neatly deposited OSE sublayer with thickness d–d_0 is actually so thick (>30 nm) that simple quantum mechanical tunnelling through it is not a viable possibility. Although the detailed physical picture is lacking, we nevertheless assume that there exists a potential barrier for spin injection at the Co/OSE interface (Fig. 1c), which may be self-adjusted[7]. Once carriers are injected through this interface they easily reach the neat sublayer, where they drift under the influence of the electric field towards the other

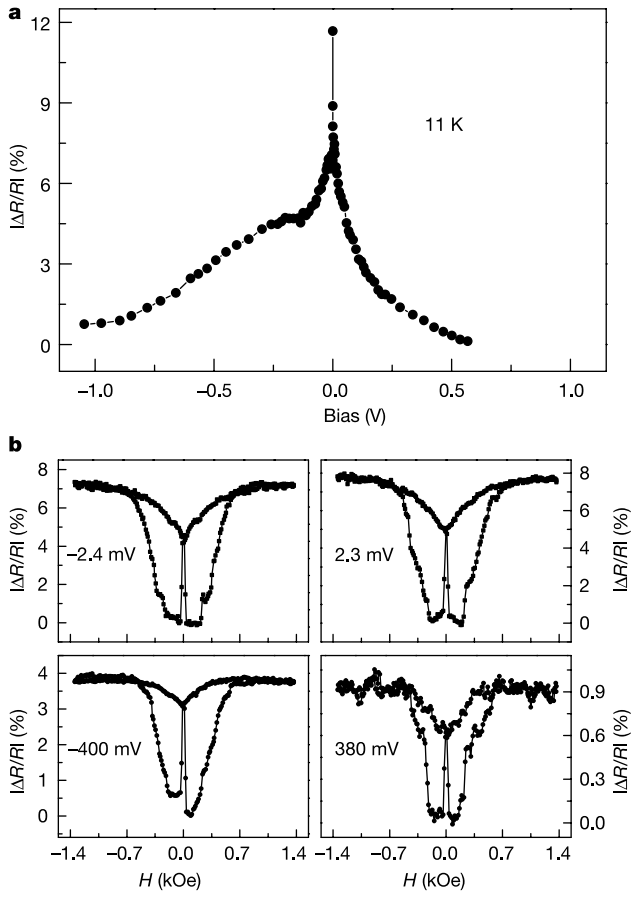

Figure 3 Bias voltage dependence. **a**, $|\Delta R/R|$ for a LSMO/Alq_3/Co device with $d = 160$ nm measured at 11 K, as a function of V. **b**, Spin-valve related GMR loops at four different V values.

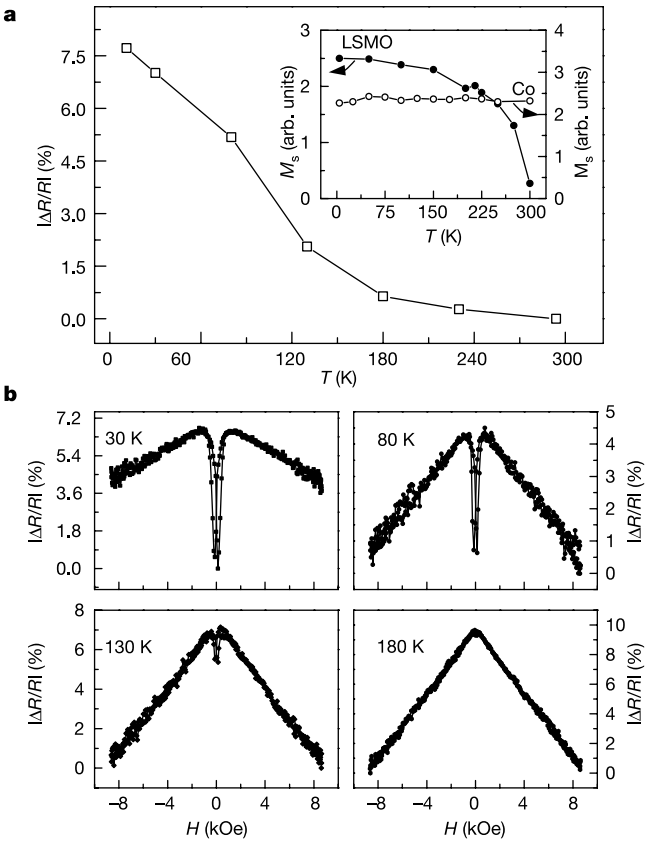

Figure 4 Temperature dependence. **a**, $|\Delta R/R|$ measured at $V = 2.5$ mV as a function of temperature for the same device as in Fig. 3. The inset shows the magnetizations of the Co and LSMO electrodes versus T, measured using MOKE. **b**, The low-field GMR hysteresis loop, and the high-field magnetoresistance measured at various temperatures as indicated. M_s, saturation magnetization.

interface, from which they can be extracted. As the injected carriers reach the end of the ill-defined sublayer, the spin polarization is p_1; it further decays in the remaining neatly deposited sublayer with a surviving probability $\exp[-(z-d_0)/\lambda_S]$, where z is the drift/diffusion distance along the normal direction to the interface, and λ_S is the spin diffusion length in the neatly deposited OSE sublayer. The spin polarization p is defined as $p=\frac{N_\uparrow-N_\downarrow}{N_\uparrow+N_\downarrow}$, where $N_\uparrow$ ($N_\downarrow$) is the carrier density in the majority (minority) spin state. We express the thickness dependence of the GMR magnitude, $\Delta R/R$, which is the maximum relative change in electrical resistance R within the spin-valve hysteresis loop, assuming no loss of spin memory at the interfaces owing to the self-adjusting capability of the OSE[7]:

$$\frac{\Delta R}{R}=\frac{R_{AP}-R_P}{R_{AP}}=\frac{2p_1p_2e^{-(d-d_0)/\lambda_s}}{1+p_1p_2e^{-(d-d_0)/\lambda_s}} \quad (1)$$

where R_{AP} and R_P denote R in the anti-parallel and parallel magnetization configurations, respectively. For inverse magnetoresistance, $R_{AP}<R_P$; therefore $\Delta R/R$ is negative, according to equation (1). We used equation (1) with three adjustable parameters, namely p_1p_2, d_0 and λ_S to fit the data for $\Delta R/R$ in Fig. 2b. The good agreement shown in Fig. 2b was obtained with the following parameters: $p_1p_2=-0.32$; $d_0=87$ nm, which is close to the lower limit of d below which the I–V response becomes linear; and $\lambda_S=45$ nm, which is a reasonable value for λ_S in the neatly deposited OSE sublayer. The obtained λ_S is smaller than what was extracted for T_6 (ref. 12), possibly owing to the aluminium element in Alq_3 that may increase the spin-orbit coupling in this OSE. However, λ_S is similar to what was extracted from spin-valve devices of single-walled carbon nanotubes[20].

We measured the dependences of $\Delta R/R$ of the organic spin-valve devices on the bias voltage V and temperature T. A series of GMR hysteresis curves for different V are displayed in Fig. 3b for the $d=160$ nm device; similar dependence was obtained in devices having other OSE thicknesses. $\Delta R/R$ strongly depends on V, as summarized in Fig. 3a; it peaks at $V\approx 0$ and decreases as the applied voltage increases. In addition, the V dependence exhibits a clear asymmetry; it decays more slowly with V for negative voltages, which is similar to what was observed in magnetic tunnel junctions with LSMO and Co or CoFe electrodes[17,21].

$\Delta R/R$ also strongly depends on T. A series of GMR hysteresis is shown in Fig. 4b; the complete temperature dependence of $\Delta R/R$ is summarized in Fig. 4a. From equation (1) the decrease of $\Delta R/R$ at high temperatures may contain two contributions. One contribution is the decreased spin polarization of the LSMO injecting electrode, p_1 at high T and the other is the decreased λ_S of the neatly deposited OSE sublayer[8]. A decrease in p_1 is expected for LSMO owing to its low Curie temperature of about 300 K (Fig. 4a, inset). The temperature dependence of $\Delta R/R$, however, does not qualitatively follow that of the magnetization of the LSMO itself; $\Delta R/R$ vanishes below the Curie temperature of the LSMO. This indicates that λ_S in Alq_3 has a stronger temperature dependence than that of the LSMO magnetization. To check this conclusion, we also fabricated a spin-valve device in which the LSMO bottom electrode was replaced by a Fe electrode having a much higher Curie temperature than LSMO. Although both FM electrodes of this device maintain their ferromagnetic properties well above room temperature, we still observed a decrease of the GMR with T, similar to that displayed in Fig. 4a. In addition, we also measured the T dependence of the spin relaxation time in Alq_3 using the spin-1/2 photoluminescence detected magnetic resonance at $g\approx 2$ as a function of temperature. We found that the spin-1/2 resonance signal decreases with T in much the same way as the decrease with T of the spin-valve GMR in our devices (Fig. 4a). This shows first, that spin-1/2 carriers in the OSE are responsible for the GMR response in our devices; and, second, that the decreased GMR at high temperatures is due to the increase of the spin relaxation rate in the OSE.

At increased T we found another interesting effect; an increase in high-field magnetoresistance (HFMR) accompanies the decrease of the low-field spin-valve related GMR (Fig. 4b). We have also observed a similar but much smaller HFMR in the LSMO film itself (Supplementary Information). However, the spin-valve device resistance is several orders of magnitude greater than that of the LSMO electrode. Therefore, the apparent HFMR cannot simply be explained by the change in the serial resistance of the LSMO electrode. Similar HFMR response was also reported in some other devices using LSMO electrodes[18]; and it can also explain the recently measured room-temperature resistance difference between two magnetic fields in planar LSMO/T_6/LSMO devices[12]. In the latter devices, the relative magnetization orientations in the two identical electrodes should not depend on H; therefore the observed magnetoresistance may be of the same origin as that of this HFMR, but is not due to the conventional spin-valve effect.

This study shows that spin-polarized carrier injection, transport and detection, which are the main ingredients of spintronics, can be successfully achieved using π-conjugated OSE. This may initiate a variety of exciting new applications in organic spintronics such as spin-OLEDs, enabled by the functionalities of the OSE. □

Received 13 November; accepted 23 December 2003; doi:10.1038/nature02325.

1. Baibich, M. N. *et al.* Giant magnetoresistance of (001)Fe/(001)Cr magnetic superlattices. *Phys. Rev. Lett.* **61,** 2472–2475 (1988).
2. Moodera, J., Kinder, L., Wong, T. & Meservey, R. Magnetic tunnel junction. *Phys. Rev. Lett.* **74,** 3273–3276 (1995).
3. Wolf, S. A. *et al.* Spintronics: a spin-based electronics vision for the future. *Science* **294,** 1488–1495 (2001).
4. Kikkawa, J. M. & Awschalom, D. D. Lateral drag of spin coherence in gallium arsenide. *Nature* **397,** 139–141 (1999).
5. Ohno, Y. *et al.* Electrical spin injection in a ferromagnetic semiconductor heterostructure. *Nature* **420,** 790–792 (1999).
6. Hanbicki, A. T. *et al.* Efficient electrical spin injection from a magnetic metal/tunnel barrier contact into a semiconductor. *Appl. Phys. Lett.* **80,** 1240–1242 (2002).
7. Xie, S. J., Ahn, K. H., Smith, D. L., Bishop, A. R. & Saxena, A. Ground-state properties of ferromagnetic metal/conjugated polymer interfaces. *Phys. Rev. B* **67,** 125202 (2003).
8. Krinichnyi, V. I. 2-mm waveband electron paramagnetic resonance spectroscopy of conducting polymers. *Synth. Met.* **108,** 173–222 (2000).
9. Friend, R. H. *et al.* Electroluminescence in conjugated polymers. *Nature* **397,** 121–128 (1999).
10. Forrest, S., Burrows, P. & Thompson, M. The dawn of organic electronics. *IEEE Spectr.* **37,** 29–34 (2000).
11. Voss, D. Cheap and cheerful circuits. *Nature* **407,** 442–444 (2000).
12. Dediu, V., Murgia, M., Matacotta, F. C., Taliani, C. & Barbanera, S. Room temperature spin polarised injection in organic semiconductor. *Solid State Commun.* **122,** 181–184 (2002).
13. Bowen, M. *et al.* Nearly total spin polarization in $La_{2/3}Sr_{1/3}MnO_3$ from tunneling experiments. *Appl. Phys. Lett.* **82,** 233–235 (2003).
14. Lee, S. T., Hou, X. Y., Mason, M. G. & Tang, C. W. Energy level alignment at AlQ/metal interfaces. *Appl. Phys. Lett.* **72,** 1593–1595 (1998).
15. Arisi, E. *et al.* Organic light emitting diodes with spin polarized electrodes. *J. Appl. Phys.* **93,** 7682–7683 (2003).
16. Dieny, B. *et al.* Giant magnetoresistance of magnetically soft sandwiches: dependence on temperature and on layer thicknesses. *Phys. Rev. B* **45,** 806–813 (1992).
17. De Teresa, J. M. *et al.* Inverse tunnel magnetoresistance in $Co/SrTiO_3/La_{0.7}Sr_{0.3}MnO_3$: new ideas on spin-polarised tunnelling. *Phys. Rev. Lett.* **82,** 4288–4291 (1999).
18. De Teresa, J. M. *et al.* Role of metal-oxide interface in determining the spin polarization of magnetic tunnel junctions. *Science* **286,** 507–509 (1999).
19. Jullière, M. Tunneling between ferromagnetic films. *Phys. Lett. A* **54,** 225–226 (1975).
20. Tsukagoshi, K., Alphenaar, B. W. & Ago, H. Coherent transport of electron spin in a ferromagnetically contacted carbon nanotube. *Nature* **401,** 572–574 (1999).
21. Hayakawa, J. *et al.* The origin of bias-dependence in $CoFe/SrTiO_3/La_{0.7}Sr_{0.3}MnO_3$ magnetic tunnel junctions. *J. Appl. Phys.* **91,** 8792–8794 (2002).

Supplementary Information accompanies the paper on **www.nature.com/nature**.

Acknowledgements We thank X.G. Li at the University of Science and Technology of China for providing the LSMO films and C. Taliani, V. Dediu, V. Burtman and D. Smith for discussions. We also thank F. J. Wang, C. G. Yang, C. Z. Liu and M. DeLong for assistance with the measurements. This work was supported in part by the National Science Foundation, Petroleum Research Foundation, DARPA, and the Department of Energy.

Competing interests statement The authors declare that they have no competing financial interests.

Correspondence and requests for materials should be addressed to J.S. (jshi@physics.utah.edu).